Magnetic phase diagram of the one-band Hubbard Hamiltonian with application to high-T_c superconducting oxides

Weiyi Zhang, M. Avignon,* and K. H. Bennemann
Institute for Theoretical Physics, Freie Universität Berlin, Arnimallee 14, D-1000 Berlin 33, Federal Republic of Germany
(Received 22 October 1990; revised manuscript received 12 November 1991)

Using an extension of the Gutzwiller approximation and applying the Bethe-lattice method, we have studied the magnetic phase transition between various phases of one-band Hubbard Hamiltonian. We allow the magnetic moments to point in an up or down direction and determine self-consistently the local magnetic moment on each lattice site. We obtain that the paramagnetic state with local moments is energetically more favorable than the Pauli paramagnetic state. The phase transition from magnetically ordered to disordered states involves mainly a transition to a paramagnetic state with local moments. We calculated the magnetic phase diagram as function of on-site Coulomb repulsion U and dopant concentration δ. Results are discussed in connection with the phase diagram observed for high-T_c superconductors. In agreement with experiment, we obtain, for reasonably large values of U, a small critical dopant concentration of 3-5% for the destruction of antiferromagnetism *due to the occurrence of a paramagnetic state with local moments.* We show that the Hartree-Fock approximation greatly exaggerates the stability of magnetic states. The validity of our results is discussed.

I. INTRODUCTION

Since the discovery of high-T_c superconductors five years ago,[1,2] many studies were carried out both experimentally and theoretically. Several physical properties have been well established experimentally, in particular, the magnetic phase diagram.[3,4] By now it is clear that correlations and magnetic fluctuations play an important role in these materials.[5–12] For example, this is indicated by the insulating and antiferromagnetic phases in the half filled case, as well as by the photoemission spectra. The experimental phase diagram shows that the antiferromagnetic phase for the hole-doped system is very sensitive to the effective dopant concentration, which is induced by substitution and oxygen vacancies. Antiferromagnetism is destroyed already for dopant concentrations of 2–4 %.[3,4] The resulting paramagnetic state exhibits very strong short-range spin correlations.[13] It behaves like a spin-glass phase rather than a momentless Pauli paramagnetic state.

In order to describe the normal-state properties of the strongly correlated system, one usually applies the Hubbard Hamiltonian.[14,6] The electrons form a narrow energy band resulting from hopping between the Wannier states of neighboring lattice sites, with repulsive interaction between two electrons of opposite spins on the same lattice site. The physical properties of the Hubbard model are expected to be important for understanding the mechanism responsible for high-T_c superconductivity.[5,6] Although the Hubbard Hamiltonian is simple in form, it cannot be solved exactly, except in one dimension. Therefore, various approximate techniques have been developed. Among these, the Hartree-Fock approximation (HFA), Green's-function decoupling scheme,[14] the Gutzwiller variational approximation,[15] and the slave-boson method[16–21] have most frequently been used. The slave-boson method was developed by Coleman[16] and by Barnes[17] among others in the study of heavy-fermion systems. As shown by Kotliar and Ruckenstein[18] (KR), the Gutzwiller approximation can be obtained from the slave-boson method as a mean-field limit, the so-called saddle-point approximation. Zou and Anderson[19] have demonstrated the physical meaning of the slave-boson technique in the derivation of neutral fermion spectrum in the resonating valence bond state. However, Rasul and Li[20] found that the contributions from transverse spin fluctuation are missing when they used the KR formulation of the slave-boson method to calculate the spin-fluctuation contribution to the specific heat in the Hubbard Hamiltonian. It was realized by Li, Wölfle, and Hirschfeld[21] that the KR formulation is not spin rotation invariant in boson space because of the assumption of a spin-quantization axis. This is expected to lead to errors for studies involving spin dynamics and fluctuations and furthermore might also lead to errors in mean-field calculation where the spin-quantization axis is spatially nonuniform. Therefore, the validity of the KR slave-boson mean-field model might be questionable. However, recently several groups[22,23] made comparative studies of the KR slave-boson mean-field model and quantum Monte Carlo calculations for the dimensions $D=2$ and 3 Hubbard models, and excellent agreement is obtained for the ground-state energy and local quantities for both paramagnetic and the antiferromagnetic phases. The paramagnetic and antiferromagnetic ground-state energies calculated in the KR slave-boson mean-field approximation have also been shown by Metzner and Vollhardt[24] to be the exact result in the limit of infinite dimensions. Therefore, one can also study the effect of dimensionality on the validity of the slave-boson mean field by expanding around $D=\infty$, using $(1/D)$ as small parameter. Results for self-energy[25] are available for the one-band Hub-

bard Hamiltonian in the weak-coupling limit. While for $D=1$, no agreement with the $D=\infty$ mean-field result is obtained. For $D=3$, one finds very good agreement. Also, for $D=2$, one finds reasonably good agreement with the $D=\infty$ mean-field results. Similar calculations for the Anderson Hamiltonian also confirm this trend.[26] All these studies show that the KR slave-boson mean-field calculations yield very good results for the ground-state properties for dimensions $D \geq 2$.

That the phase diagram does not depend sensitively on the dimensionality for $D \geq 2$, can be understood as follows. The slave-boson mean-field discussed above is a local approximation. The dimensionality is implicitly contained in the shape of the density of states (DOS), since this is the only quantity that is involved in the minimization of the ground-state energy. Thus, by properly scaling the energy parameters, the magnetic phase diagram does not depend sensitively on the shape of the density of states, since for the energy minimization, only integrals over the density of states occur. This can be also seen from the calculation of Kotliar and Ruckenstein.[18] Of course, the phase boundaries will shift somewhat as the dimension changes from $D=2$ to 3 due to the van Hove singularity in two dimension, but the overall feature of the magnetic phase diagram will remain the same. This discussion suggests the use of the KR slave-boson mean-field approximation for determining the magnetic phase diagram. This should then yield reliable results for $D \geq 2$.

Using a slave-boson mean-field treatment, many calculations have been performed for the Hubbard or extended Hubbard Hamiltonian.[22–25,27–29] So far, all calculations have assumed translational symmetry in real space, which limits these studies to ordered magnetic states. Hence, magnetic transitions consist of a transition from a ferromagnetic or an antiferromagnetic state to a Pauli paramagnetic state. Furthermore, one obtains a large discrepancy with experiment for the doping dependence of the antiferromagnetic state. The experimental results show that the antiferromagnetic state is destroyed for dopant concentration of 2–4%, while the slave-boson mean-field model yields a critical dopant concentration, about 15% for typical Hamiltonian parameters. This discrepancy is expected, since the translational symmetry excludes the spin disordered states. Note that without using the translational symmetry, one expects the paramagnetic state with local moments existing on every lattice site and having random directions to be the more realistic paramagnetic state. It is well known that the Pauli paramagnetic state underestimates the entropy of the system. Thus, it overestimates the antiferromagnetic transition temperature.

In this paper, we use the Hubbard Hamiltonian and apply the slave-boson mean-field approximation. We do not assume translational symmetry and include properly the on-site charge fluctuations and the occurrence of local magnetic moments on every lattice sites. This requires a theoretical treatment extending previous studies using the slave-boson method. To determine the electronic Green's functions and the density of states, we apply the Bethe-lattice method in real space, which has been successfully used for the study of alloys.[30] In the diagrammatic expansion of real lattices, the first and often the only set of diagrams that can be summed are the tree diagrams that correspond to a Bethe lattice. This approximation consists in choosing only self-retracing paths.[31–32] Van Dongen and Vollhardt[33] have shown that the phase diagram obtained from the Bethe-lattice structure qualitatively agrees with those for a hypercubic lattice in $D=\infty$ for a simplified Hubbard model in which only one kind of spin is allowed to hop.

Using a slave-boson mean-field approximation, we studied extensively the relative stability of various ordered states like antiferromagnetic, ferromagnetic, and Pauli paramagnetic state. We also consider a paramagnetic phase in which local moments are assumed to exist on each site, as in the magnetically ordered phases. Localized moments in transition metal alloys have been discussed before by Engelsberg, Brinkman, and Doniach,[34] Wang, Evanson, and Schrieffer,[35] and Zuckermann.[36] The disordered phase has been, in the past, extensively studied in the Hartree-Fock approximation[37–41] and is sometimes referred to as a spin glass. It is interesting to note that, in the context of high-T_c superconductivity, the relationship of this disordered local-moment phase to an average picture of the resonating valence bond state has been pointed out.[42] We obtain that the phase boundary from the antiferromagnetic state to the paramagnetic state is significantly shifted to a lower dopant concentration (with respect to half filling). This results from the presence of the paramagnetic state with local magnetic moments, which is energetically more favorable than the Pauli paramagnetic state, as has been obtained previously in Hartree-Fock studies of itinerant magnetism.[37–41] However, comparing with Hartree-Fock results, we find that the phase space for the magnetically ordered states is drastically reduced as a function of the dopant concentration when the correlations are properly taken into account. *A priori*, it could be expected that the remaining charge fluctuations not yet included in the slave-boson mean-field treatment could affect the magnetic phase diagram. The effect of Gaussian quantum fluctuations beyond the slave-boson mean-field theory has been considered recently by perturbation expansion in the Kotliar-Ruckenstein representation.[43,44] The discussion of the magnetic instabilities essentially depends on the structure of the unperturbed correlation function. These fluctuations are essential for describing dynamical properties, such as spin dynamics or photoemission experiments, but we are concerned here with static properties in the ground state. Recent calculations by Ferrer *et al.*[45] including charge fluctuations beyond the Hartree-Fock approximation by self-consistent second-order perturbation theory indicates, however, good agreement with the slave-boson mean-field results, as well as Monte Carlo calculations.[22,23]

In Sec. II, we first discuss the slave-boson method in the mean-field approximation, i.e., Gutzwiller variational approximation by Kotliar and Ruckenstein,[18] and derive the energy functional. Then, following Liu,[38] we apply the Bethe-lattice method for determining the electronic Green's function. This yields the density of state, which

is then used to calculate the energy. In Sec. III, results for magnetic phase diagrams and the antiferromagnetic (AF) stability energy at half filling are presented. Especially, the role of the paramagnetic state with local magnetic moments is demonstrated. Conclusions are presented in Sec. IV.

II. THEORY

The one-band Hubbard Hamiltonian is given by

$$H=\sum_{(ij),\sigma} tc_{i\sigma}^{\dagger}c_{j\sigma}+\sum_{i} Un_{i\uparrow}n_{i\downarrow} . \tag{1}$$

In order to treat correlation effects in the ground state, one introduces the four auxiliary boson operators e_i, $s_{i\sigma}$, and d_i which refer to the empty state, the singly occupied state with a spin up or down, and the doubly occupied state. Therefore, all the charge fluctuations of the single site are taken into account properly. In this mixed fermion and boson space, two constraints have to be satisfied in order to make a one-to-one correspondence between the new and old Hamiltonian in the original physical space. These are

$$c_{i\sigma}^{\dagger}c_{i\sigma}=s_{i\sigma}^{\dagger}s_{i\sigma}+d_i^{\dagger}d_i \tag{2a}$$

and

$$e_i^{\dagger}e_i+s_{i\uparrow}^{\dagger}s_{i\uparrow}+s_{i\downarrow}^{\dagger}s_{i\downarrow}+d_i^{\dagger}d_i=1 . \tag{2b}$$

By introducing Lagrange multipliers to take into account the above constraints, one arrives at the following Hamiltonian in the mixed fermion and boson space:

$$H=-\sum_{i,\sigma}\sigma\Delta_i c_{i\sigma}^{\dagger}c_{i\sigma}+\sum_{(ij),\sigma} tq_{i\sigma}q_{j\sigma}c_{i\sigma}^{\dagger}c_{j\sigma} +\sum_{i} Ud_i^{\dagger}d_i+\sum_{i,\sigma}\sigma\Delta_i(s_{i\sigma}^{\dagger}s_{i\sigma}+d_i^{\dagger}d_i) . \tag{3a}$$

Here, the Δ's are the Lagrange multipliers introduced to satisfy the above constraint, Eq. (2a). The operator $q_{i\sigma}$ is given by

$$q_{i\sigma}=(1-d_i^{\dagger}d_i-s_{i\sigma}^{\dagger}s_{i\sigma})^{-1/2}(e_i^{\dagger}s_{i\sigma}+s_{i\bar{\sigma}}^{\dagger}d_i)(1-e_i^{\dagger}e_i-s_{i\bar{\sigma}}^{\dagger}s_{i\bar{\sigma}})^{-1/2} . \tag{3b}$$

In the mean-field approximation, all the bosonic operators are treated as numbers. Furthermore, one can eliminate the numbers e_i, $s_{i\uparrow}$, $s_{i\downarrow}$, using the constraints given by Eq. (2). One then obtains the Gutzwiller variational approximation, which corresponds to a minimization problem of E with respect to Δ_i and d_i^2:

$$E=\frac{1}{N}\langle H_{\text{eff}}\rangle+\frac{1}{N}\sum_{i} Ud_i^2+\frac{1}{N}\sum_{i,\sigma}\sigma\Delta_i\langle c_{i\sigma}^{\dagger}c_{i\sigma}\rangle . \tag{4a}$$

Here, H_{eff} is the modified effective single-particle Hamiltonian

$$H_{\text{eff}}=-\sum_{i,\sigma}\sigma\Delta_i c_{i\sigma}^{\dagger}c_{i\sigma}+\sum_{(ij),\sigma} tq_{i\sigma}q_{j\sigma}c_{i\sigma}^{\dagger}c_{j\sigma} , \tag{4b}$$

with

$$q_{i\sigma}^2=\frac{1}{n_{i\sigma}(1-n_{i\sigma})}\{[(1-n_i+d_i^2)(n_{i\sigma}-d_i^2)]^{1/2}+[d_i^2(n_i-n_{i\sigma}-d_i^2)]^{1/2}\}^2 . \tag{4c}$$

N denotes the total number of lattice sites. $n_{i\sigma}$ is the occupation number at site i with spin index σ, $n_i=n_{i\uparrow}+n_{i\downarrow}$, and $d_i^2=\langle n_{i\uparrow}n_{i\downarrow}\rangle$ denotes the double occupation. The Lagrange multipliers Δ_i and double occupation numbers d_i^2 are, in principle, site dependent. These parameters Δ_i play the role of exchange fields determined self-consistently for the different phases in contrast with HFA where $\Delta_i=U(n_{i\uparrow}-n_{i\downarrow})/2$. In solving the subsequent equation for the Green's function, one usually assumes translational symmetry and thus neglects any magnetic disordered states in the system.

Previous HFA studies[37–41] have shown that, in certain parameter ranges, the system does not want to stay in these magnetically long-range ordered states. For a given orientation of the moment at a site, neighboring moments may point up or down with respect to the z direction. The proper moment configuration is determined by the energy of the system. We introduce the probability r for the neighboring moments to point in the same direction. s gives the probability for the neighboring moments to point in opposite direction. Thus, $r+s=1$. Within this approximation, $r=1$ corresponds to a ferromagnetic state and $r=0$ to an antiferromagnetic state. All other values of r correspond to some sort of short-range ordering, except $r=0.5$, which refers to a generalized paramagnetic state. This coincides with the Pauli paramagnetic state if the on-site moment is zero. Note that by applying the Bethe-lattice method to the slave-boson theory we are also able to include approximately magnetically disordered states. This approximation should produce a more realistic magnetic phase diagram than obtained in previous studies, for example, using translational symmetry.[28,29]

To obtain the energy functional, Eq. (4), we first calcu-

late the contribution resulting from H_{eff}. We introduce the *retarded* Green's function

$$G_{(ij)\sigma}(t)=-i\theta(t)\langle[c_{i\sigma}(t),c_{j\sigma}^{\dagger}(0)]_{+}\rangle , \tag{5}$$

where $\theta(t)$ is a step function. The Green's function satisfies the following equation of motion:

$$(\omega+\sigma\Delta_i)G_{(ij)\sigma}(\omega)=\delta_{ij}+\sum_{l(\neq i)} tq_{i\sigma}q_{l\sigma}G_{(lj)\sigma}(\omega) . \tag{6}$$

Since every site has either a moment pointing up or down ($\Delta_i>0$, $\Delta_i<0$), we will use $+,-$ to denote these two directions. Therefore, the diagonal Green's function at the origin satisfies

$$(\omega+\sigma\Delta)G_{(00)\sigma}^{++}(\omega)=1+zt[rq_{\sigma}q_{\sigma}G_{(10)\sigma}^{++}(\omega)+sq_{\sigma}q_{\bar{\sigma}}G_{(10)\sigma}^{-+}(\omega)] , \tag{7a}$$

$$(\omega-\sigma\Delta)G_{(00)\sigma}^{--}(\omega)=1+zt[rq_{\bar{\sigma}}q_{\bar{\sigma}}G_{(10)\sigma}^{--}(\omega)+sq_{\bar{\sigma}}q_{\sigma}G_{(10)\sigma}^{+-}(\omega)] . \tag{7b}$$

The sign of the exchange energy for an electron with spin σ depends on the local-moment direction. The exchange energy is denoted by $\sigma\Delta$ for site with the moment pointing in up direction and by $-\sigma\Delta$ for site with the moment pointing in down direction. z is number of nearest neighbors, 0 and 1 stand for the origin and first neighbor to the origin. q_{σ} is the band narrowing factor due to the on-site Coulomb repulsion. Since $q_{\sigma}^{-}=q_{\bar{\sigma}}^{+}$, we have dropped the superscript $\pm$ and expressed all the band narrowing factors in terms of the quantities of moment-up state from now on. In the Bethe-lattice method one defines the following transfer matrix

$$T_{\sigma}^{ij}=\frac{G_{(10)\sigma}^{ij}}{G_{(00)\sigma}^{jj}} . \tag{8}$$

Thus, one can write the on-site Green's function in terms of their transfer matrix

$$G_{(00)\sigma}^{++}=\frac{1}{\omega+\sigma\Delta-zt(rq_{\sigma}q_{\sigma}T_{\sigma}^{++}+sq_{\sigma}q_{\bar{\sigma}}T_{\sigma}^{-+})} , \tag{9a}$$

$$G_{(00)\sigma}^{--}=\frac{1}{\omega-\sigma\Delta-zt(rq_{\bar{\sigma}}q_{\bar{\sigma}}T_{\sigma}^{--}+sq_{\bar{\sigma}}q_{\sigma}T_{\sigma}^{+-})} . \tag{9b}$$

The assumption made in the Bethe-lattice method is that the transfer matrix is independent of the lattice, this is equivalent to assuming a certain profile for the density of state. By deriving the equation of motion for the Green's function $G_{(10)\sigma}^{++}$, etc., on the right-hand side of Eq. (7) one obtains for the transfer matrix the equations

$$(\omega+\sigma\Delta)T_{\sigma}^{++}(\omega)=tq_{\sigma}q_{\sigma}+(z-1)t[rq_{\sigma}q_{\sigma}T_{\sigma}^{++}T_{\sigma}^{++}(\omega)+sq_{\sigma}q_{\bar{\sigma}}T_{\sigma}^{-+}T_{\sigma}^{++}(\omega)] , \tag{10a}$$

$$(\omega-\sigma\Delta)T_{\sigma}^{-+}(\omega)=tq_{\bar{\sigma}}q_{\sigma}+(z-1)t[rq_{\bar{\sigma}}q_{\bar{\sigma}}T_{\sigma}^{--}T_{\sigma}^{-+}(\omega)+sq_{\bar{\sigma}}q_{\sigma}T_{\sigma}^{+-}T_{\sigma}^{-+}(\omega)] , \tag{10b}$$

$$(\omega+\sigma\Delta)T_{\sigma}^{+-}(\omega)=tq_{\sigma}q_{\bar{\sigma}}+(z-1)t[rq_{\sigma}q_{\sigma}T_{\sigma}^{++}T_{\sigma}^{+-}(\omega)+sq_{\sigma}q_{\bar{\sigma}}T_{\sigma}^{-+}T_{\sigma}^{+-}(\omega)] , \tag{10c}$$

$$(\omega-\sigma\Delta)T_{\sigma}^{--}(\omega)=tq_{\bar{\sigma}}q_{\bar{\sigma}}+(z-1)t[rq_{\bar{\sigma}}q_{\bar{\sigma}}T_{\sigma}^{--}T_{\sigma}^{--}(\omega)+sq_{\bar{\sigma}}q_{\sigma}T_{\sigma}^{+-}T_{\sigma}^{--}(\omega)] . \tag{10d}$$

We use the simpler average procedure for the transfer matrix that has been used previously.[38] For not too small z, the difference between this and a more sophisticated scheme can be neglected. Furthermore, one can simplify the result by introducing the following transformations:

$$\eta_{\sigma}=rq_{\sigma}q_{\sigma}T_{\sigma}^{++}+sq_{\sigma}q_{\bar{\sigma}}T_{\sigma}^{-+} \tag{11a}$$

and

$$\zeta_{\sigma}=rq_{\bar{\sigma}}q_{\bar{\sigma}}T_{\sigma}^{--}+sq_{\bar{\sigma}}q_{\sigma}T_{\sigma}^{+-} . \tag{11b}$$

From this one obtains the following expression for the retarded Green's function[46]

$$G_{(00)\sigma}^{++}=G_{(00)\bar{\sigma}}^{--}=\frac{1}{\omega+\sigma\Delta-zt\eta_{\sigma}} , \tag{12}$$

with η_{σ} given by

$$\eta_{\uparrow}=\frac{rtq_{\uparrow}^{4}}{\omega+\Delta-(z-1)t\eta_{\uparrow}}+\frac{stq_{\uparrow}^{2}q_{\downarrow}^{2}}{\omega-\Delta-(z-1)t\eta_{\downarrow}} \tag{13a}$$

and

$$\eta_{\downarrow}=\frac{rtq_{\downarrow}^{4}}{\omega-\Delta-(z-1)t\eta_{\downarrow}}+\frac{stq_{\downarrow}^{2}q_{\uparrow}^{2}}{\omega+\Delta-(z-1)t\eta_{\uparrow}} . \tag{13b}$$

Using this Green's function one can calculate the density of states

$$N_{\sigma}(\omega)=-\frac{1}{\pi}\mathrm{Im}G_{(00)\sigma}^{++}(\omega) , \tag{14a}$$

the average electron number per lattice site

$$n_{\sigma}=\int_{-\infty}^{E_F}N_{\sigma}(\omega)d\omega , \tag{14b}$$

and the total energy

$$E=\sum_{\sigma}\left[\int_{-\infty}^{E_F}\omega N_{\sigma}(\omega)d\omega+\sigma\Delta n_{\sigma}\right]+Ud^2 . \quad (14c)$$

As usual, the Fermi energy is determined from the total number of electrons in the system. For a fixed parameter r, one has to minimize the total energy of the system self-consistently with respect to the variables d and Δ.

For the states with translational invariance, one can get the full analytical expression for the Green's function,[38,47]

$$G_{(00)}(\omega)=\frac{(z-2)\omega-zi[4(z-1)q^2t^2-\omega^2]^{1/2}}{2(z^2q^2t^2-\omega^2)} \quad (15a)$$

for the Pauli paramagnetic state,

$$G_{(00)\sigma}(\omega)=\frac{2(z-1)}{(z-2)(\omega+\sigma\Delta)+zi[4(z-1)q_{\sigma}^4t^2-(\omega+\sigma\Delta)^2]^{1/2}} \quad (15b)$$

for ferromagnetic state, and

$$G_{(00)\sigma}(\omega)=\frac{2(z-1)(\omega-\sigma\Delta)}{(z-2)(\omega^2-\Delta^2)+zi\{(\omega^2-\Delta^2)[4(z-1)q_{\sigma}^2q_{\bar{\sigma}}^2t^2-(\omega^2-\Delta^2)]\}^{1/2}} \quad (15c)$$

for antiferromagnetic state. From Eq. (15a), it is clear that the half bandwidth in the noninteraction system is $E_B=2t\sqrt{(z-1)}$. Note that $z\to\infty$ and keeping $\sqrt{z}t$ finite reproduces the elliptic density of states commonly used as a model density of states.

In summary then, we determine the density of states from Eq. (14a), the magnetic moment from $\mu=n_{\uparrow}-n_{\downarrow}$, and the total energy from Eq. (14c).

III. RESULTS

We have performed numerical calculations for three magnetic phases. With $r=1$, we determine the ferromagnetic (FM) state, with $r=0.5$ the paramagnetic state with local moments (LMP), and with $r=0$ the antiferromagnetic state (AF). It should be mentioned that the states with $r\neq 0.5$ have some short-range magnetic moment ordering. If $r>0.5$ this short-range magnetic ordering is ferromagnetic like. If $r<0.5$ this short-range magnetic ordering is antiferromagneticlike. To demonstrate the significance of the LMP state, we concentrate here on the state without short-range ordering, i.e., $r=0.5$. We obtain that the transition from a magnetically ordered state to a disordered state involves mainly a paramagnetic state with local moments. Once the LMP state is included, the stability of the antiferromagnetic state is drastically reduced with increasing dopant concentration. To minimize the errors introduced by the simple averaging of the transfer matrix with respect to the moment configuration, we use for the coordination number of the Bethe-lattice $z=12$. Results for different values of z can be deduced from the ones for $z=12$, since the presented results are nearly scaled by the half bandwidth $E_B=2t\sqrt{z-1}$ and will not depend crucially on z.

In Fig. 1 the phase diagram for the transitions from the antiferromagnetic (AF) to the Pauli paramagnetic (Pauli-PM) state is shown. It should be noted that the onsite Coulomb repulsion U is scaled by the half bandwidth $E_B=2t\sqrt{z-1}$. One sees that the maximum dopant concentration ($\delta=1-n$) at which the phase transition occurs is less than 0.2, the phase boundary changes rapidly for small U and becomes almost vertical for $U>30E_B$.

With regard to the transition from AF to Pauli PM our result is almost the same as the one by Kotliar and Ruckenstein,[18] as can be seen by scaling the energy parameters by half bandwidth. This indicates that the slave-boson mean-field phase diagram does not depend sensitively on the form of the density of states. Our result can also be compared with the one for $D=\infty$ calculated by Fazekas, Menge, and Müller-Hartmann.[48] It is seen that the overall features of the phase diagram are very similar. The $U\to\infty$ limit of AF–Pauli-PM boundary is $\delta_c\simeq 0.1$, a value close to that obtained by Fazekas, Menge, and Müller-Hartmann,[48] while Metzner and Vollhardt[24] reported a slightly larger value $\delta_c\simeq 0.15$. Due to the

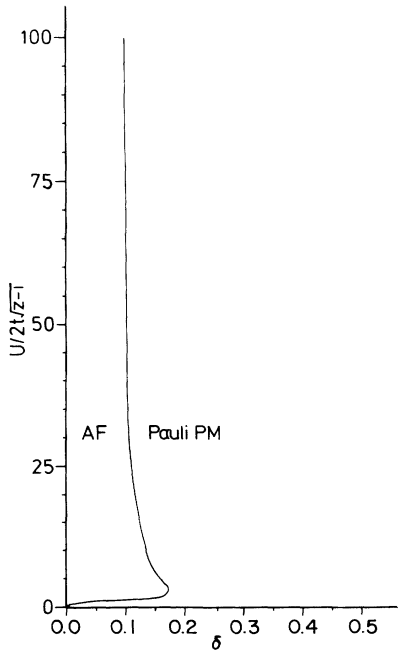

FIG. 1. Phase diagram for the transition between Pauli paramagnetic (Pauli-PM) phase and antiferromagnetic (AF) phase using a one-band Hubbard Hamiltonian. The doping concentration is $\delta=1-n$ and U is scaled by half the bandwidth ($E_B=2t\sqrt{z-1}$).

particle-hole symmetry, the other half of the phase diagram can be easily obtained by making a mirror reflection along the U axis.

In Fig. 2 we present the phase diagram for transitions from ferromagnetic (FM) to Pauli paramagnetic states. Our result is very similar to the one obtained by Kotliar and Ruckenstein[18] for $U > 15E_B$. For smaller values of U, we obtain rather different results. In our case the ferromagnetic state is still stable with respect to the Pauli paramagnetic state for $8E_B < U < 15E_B$ and for small-dopant concentration. However, the stability energy for ferromagnetism in this region is very small. The phase transition in this region might be of first order and thus it would not have been obtained by Kotliar and Ruckenstein, since their method used is only valid for a second-order phase transition. A comparison with results for $D = \infty$ (Ref. 48) shows that the overall features of the phase diagram are very similar, except for the small-dopant-concentration region and $8E_B < U < 15E_B$.

In Fig. 3 we show results for the interesting third-phase transition from the paramagnetic state with local moments (LMP) to the Pauli paramagnetic state. The LMP state develops at somewhat higher values of U and lies in between the antiferromagnetic and ferromagnetic phase boundaries. As can be deduced from Fig. 1 and Fig. 3, the LMP–Pauli-PM phase boundary crosses the AF–Pauli-PM phase boundary at the point $U = 5E_B$ and $\delta = 0.16$ and becomes linear for larger values of U and approaches asymptotic $\delta \approx 0.3$ parallel to the U axis. One sees further from Fig. 2 and Fig. 3, that this LMP–Pauli-PM phase boundary also crosses the FM–Pauli-PM phase boundary at $U \simeq 75E_B$. We would like to emphasize that this phase is a homogeneous random moments phase and has lower energy for most of the phase space. We will see later that this LMP phase may explain the occurrence of a spin-glass state after the destruction of antiferromagnetism in the hole-doped high-T_c superconductors.

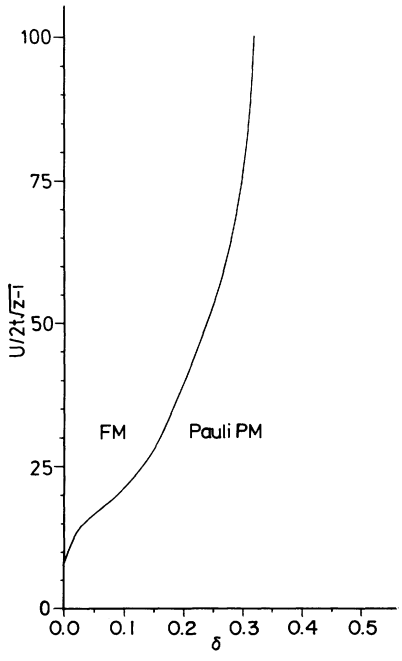

FIG. 2. Phase diagram for the transition between Pauli paramagnetic (Pauli-PM) phase and ferromagnetic (FM) phase for the one-band Hubbard Hamiltonian.

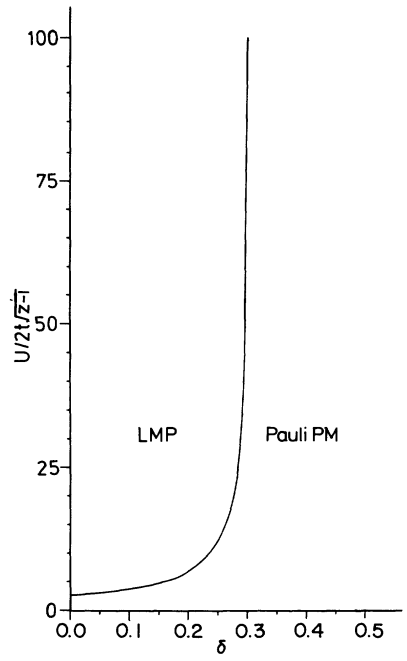

FIG. 3. Phase diagram for the transition between Pauli paramagnetic (Pauli-PM) phase and paramagnetic phase with local magnetic moments (LMP) for the one-band Hubbard Hamiltonian.

In Fig. 4 we show the total phase diagram obtained from combining the results shown in Figs. 1–3. The phase diagram is determined by comparing the energies of the different phases. One of the most interesting results is that the antiferromagnetism is drastically reduced due to the existence of the LMP state. For $U \geq 30E_B$, the antiferromagnetic state seems to be stable only in the vicinity of half-band filling. Note, that for small values of $U < 5E_B$, the system still stays in the antiferromagnetic state up to $\delta = 0.17$. The situation changes significantly for moderately larger U values. One sees, that the antiferromagnetic state is restricted to a very small-dopant concentration, range from 3 to 5% for $U = (7-10)E_B$. For increasing U (or δ) the LMP state quickly becomes energetically more favorable than the antiferromagnetic state. Also, the ferromagnetic phase gets changed by LMP state. The LMP state pushes the ferromagnetic state to very high values of U, as can be seen by comparing with Fig. 2. Note, that in the lower part of the phase diagram ($U < 10E_B, 0 < \delta < 0.3$) as shown in the insert of Fig. 4, the LMP state in our calculation occurs in almost the same range of δ as the ferromagnetic phase calculated by Fazekas, Menge, and Müller-Hartmann.[48] For large U, the system first changes as function of δ fom the LMP state to the ferromagnetic state, then to a Pauli paramagnetic state. For $U \rightarrow \infty$, the tendency towards ferromag-

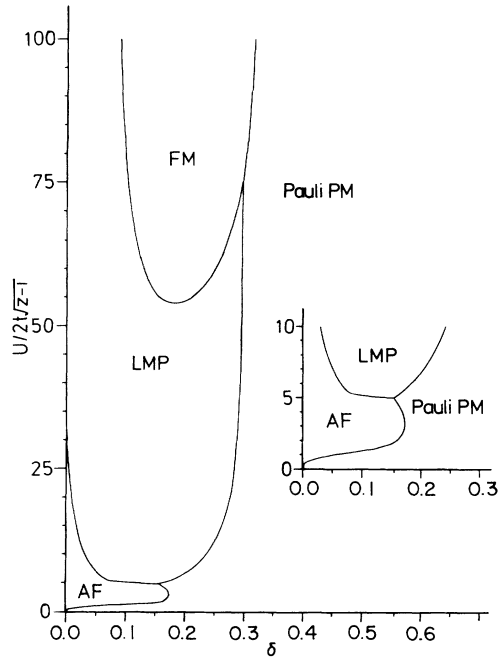

FIG. 4. The phase diagram obtained from comparison of the energy for the various phases like the antiferromagnetic (AF), the ferromagnetic (FM), the paramagnetic with local moments (LMP), and the Pauli paramagnetic (Pauli-PM). For $U \geq 30E_B$ ($E_B = 2t\sqrt{z-1}$), AF is stable only in the vicinity of half-band filling, e.g., $\delta = 0$. The inset is an enlargement of the phase diagram for smaller values of U/E_B.

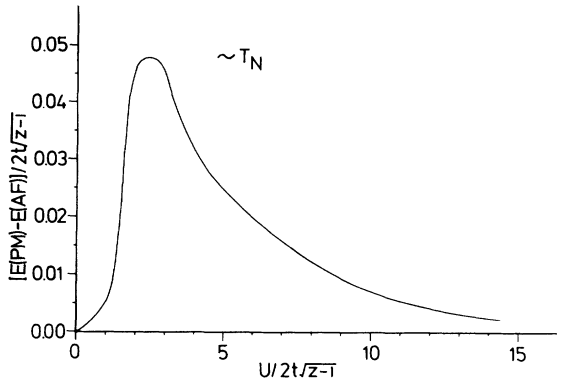

FIG. 5. The energy difference between the LMP state and the antiferromagnetic state as function of on-site Coulomb repulsion U (T_N = Néel temperature).

netic state near half-band filling is consistent with the conclusion by Nagaoka.[49]

As we discussed in the Introduction, the slave-boson mean-field calculations should yield very good results for ground-state energy and local quantities for $D \geq 2$. Dimensionality influences these results only weakly through the density of states. Therefore, we expect that the essential features of the phase diagram shown in Fig. 4 are valid for $D \geq 2$, although the exact phase boundaries might alter somewhat for $D = 2$.

Our result should also be compared with the Hartree-Fock calculations in Refs. 37–41. We see from our results that the HF approximation greatly exaggerates the stability of the magnetic states, especially, for lower average electron occupation number. The present study shows that the magnetic states exist only for doping concentration less than 0.35. The HF approximation predicts, at large U, magnetic states almost for any occupation number. As shown recently by Metzner and Vollhardt[24] that HF approximation does not yield exact results even in $D = \infty$ dimension.

The result of the energy difference in the case of half-band filling between the antiferromagnetic and LMP is shown in Fig. 5. One gets that the energy difference first increases rapidly with on-site Coulomb repulsion, then it reaches a maximum, and then decreases towards zero as $1/U$. This is a familiar result and agrees with the superexchange interaction result at large U by Anderson.[50]

From the energy difference the Néel temperature might be estimated using the well-known mean-field formula

$$E(r=0.5)-E(r=0)=0.5kT_N \ .$$

We emphasize that this is a crude estimate for the Néel temperature. In view of the used simplified band model and the Ising approximation for the local moments, we see no point in trying to improve this estimate by using more sophisticated theories of phase transition. It is interesting to note that a finite temperature slave-boson mean-field type calculation by Hasagawa[23] (including single-site fluctuation) yields similar results as shown in Fig. 5. Using

$$\Gamma \simeq 2t\sqrt{z-1}/\sqrt{3}$$

and

$$T_N/\Gamma \simeq [E(r=0.5)-E(r=0)]2\sqrt{3}/2t\sqrt{z-1}$$

(Γ = second moment of energy), one finds that Hasagawa's results for peak position and height of T_N are very close to ours. For large U, we get a smaller T_N value, which is closer to the exact ones. This is so, since for large U our paramagnetic state with local moments has lower energy than the Pauli paramagnetic state.

It is interesting to compare our results with the experimental phase diagram observed for high-T_c superconducting oxides. To fix the parameters, let us take as half bandwidth for the effective Cu square lattice[51] $E_B = 1.5$ eV and for the Coulomb interaction $U = 8E_B = 12$ eV. From our phase diagram shown in Fig. 4 we obtain a critical dopant concentration $\delta_c \simeq 0.045$, and from Fig. 5 we estimate $T_N \simeq 398$ K. These results are close to the experimental values $\delta_c = 0.02-0.04$ and $T_N \simeq 320$ K.[52] Possibly, the more interesting result is that after the antiferromagnetism destruction, we obtain a paramagnetic state with local moments on copper sites rather than a Pauli paramagnetic state. This agrees with experiments,[3,4] since local magnetic moments are a prerequisite for a spin-glass state. Our estimated value for T_N is larger than the experimentally observed one, which seems reasonable since spin fluctuations not included in the cal-

culation should further lower T_N. By comparing with experimental results for superconducting transition temperature T_c as function of δ,[53] we conclude that superconductivity occurs only when the system possesses local magnetic moments.

Including parameter values r other than $r=0.5$ would allow one to study also short-range magnetic moment ordering. The short-range magnetic ordering should resemble the antiferromagnetic one near the antiferromagnetic phase boundary and resemble the ferromagnetic one near the ferromagnetic phase boundary. These short-range ordered phases should appear near the AF-LMP, FM-LMP transition lines. As indicated in our calculation these short-range ordered phase will smooth out the transitions between these various phases, but the phase boundaries are not significantly altered.

In our paper we have restricted our study to the one-band Hubbard Hamiltonian. However, as derived by Zhang and Rice,[51] the more realistic two-band Hubbard Hamiltonian, which describes the CuO_2 plane of high-T_c superconducting oxides, can be mapped approximately into a one-band Hubbard Hamiltonian assuming $t \ll U,(\varepsilon_p-\varepsilon_d)$. This approximately holds for high-T_c superocnducting oxides. Even so the mapping to a one-band Hamiltonian might describe only approximately the various electronic properties, and we feel that the existence of local magnetic moments and the transition from antiferromagnetic to a paramagnetic state with local moments should be basically correct and also the trend for the dependence of T_N on U.

A few further critical remarks concerning the quality of the approximations used for the numerical results seem in order. First, many other studies show that for dimension $D \geq 2$, properties involving integration over the DOS are not sensitively dependent on details of DOS. Thus, similar results are obtained by using Bethe lattice approximation (adjusted to yield the proper bandwidth) and other methods. Secondly, including the remaining charge fluctuations beyond a slave-boson mean-field approximation may change somewhat our phase diagram, the stability of the antiferromagnetic phase. It might be of interest to study this more explicitly. However, comparison of our results with Monte Carlo calculation[22,23] suggests that most of the charge fluctuations are already taken care of by our slave-boson mean-field approximation.

IV. CONCLUSION

We have studied in this paper the magnetic properties of one-band Hubbard Hamiltonian, especially the magnetic transitions among the various phases that are possible. The phase diagram is obtained by comparing the energies of the different states. From this phase diagram we reach the following conclusions: the region for stable antiferromagnetic state is drastically narrowed due to the appearance of a LMP state. The transition from antiferromagnetic state to paramagnetic state is mostly a transition to a state with the local moments. For typical values U of high-T_c superconducting oxides, one can get reasonable critical dopant concentration (and rough estimate of Néel temperature). Furthermore, we find that superconductivity occurs when Cu atoms have local magnetic moments. That a state with local moments may have lower energy than a Pauli paramagnetism was already previously found.[37–41] Note, with increasing doping, itinerancy may be enhanced and thus ultimately Pauli paramagnetism may result.

ACKNOWLEDGMENTS

We would like to thank M. Garcia and S. Reindl for useful discussions. One of us (M.A.) would also like to thank the Institute for Scientific Interchange, Villa Gaulino, Torino, Italy for partial financial support. This work was supported by the Bundesministerium für Forschung und Technologie.

*Permanent address: LEPES, CNRS Grenoble, Ave. des Martyrs, F-38042 Grenoble Cedex, France.

[1] J. G. Bednorz and K. A. Müller, Z. Phys. B **64**, 189 (1986).

[2] M. K. Wu, J. R. Ashburn, C. J. Torng, P. H. Hor, R. L. Meng, L. Gao, Z. J. Huang, Y. Q. Wang, and C. W. Chu, Phys. Rev. Lett. **58**, 908 (1987).

[3] W. E. Pickett, Rev. Mod. Phys. **61**, 433 (1989).

[4] G. M. Luke *et al.*, Phys. Rev. B **42**, 7981 (1990).

[5] P. W. Anderson, Science **235**, 1196 (1987); P. W. Anderson, G. Baskaran, Z. Zou, and T. Hsu, Phys. Rev. Lett. **58**, 2790 (1987); G. Baskaran and P. W. Anderson, Phys. Rev. B **37**, 580 (1988).

[6] V. J. Emery, Phys. Rev. Lett. **58**, 2794 (1987).

[7] A. E. Ruckenstein, P. Hirschfeld, and J. Appel, Phys. Rev. B **36**, 857 (1988).

[8] M. Gabay, S. Doniach, and M. Imui, Physica C **153**, 1277 (1988).

[9] C. M. Varma, S. Schmitt-Rink, and E. Abrahams, Solid State Commun. **62**, 681 (1987).

[10] P. A. Lee and N. Read, Phys. Rev. Lett. **58**, 2691 (1987).

[11] J. E. Hirsch, Phys. Rev. Lett. **59**, 228 (1987).

[12] J. R. Schrieffer, X.-G. Wen, and S.-C. Zhang, Phys. Rev. Lett. **60**, 944 (1988); Phys. Rev. B **39**, 11 663 (1989).

[13] G. Shirane, Y. Endoh, R. Birgeneau, M. A. Kastner, Y. Hidaka, M. Oda, M. Suzuki, T. Murakami, Phys. Rev. Lett. **59**, 1613 (1987).

[14] J. Hubbard, Proc. R. Soc. London, Ser. A **276**, 283 (1963); **281**, 401 (1964).

[15] M. C. Gutzwiller, Phys. Rev. **137**, A1726 (1965).

[16] P. Coleman, Phys. Rev. B **29**, 3035 (1984).

[17] S. E. Barnes, J. Phys. F **6**, 1375 (1976); **7**, 2637 (1977).

[18] G. Kotliar and A. E. Ruckenstein, Phys. Rev. Lett. **57**, 1362 (1986).

[19] Z. Zou and P. W. Anderson, Phys. Rev. B **37**, 627 (1988).

[20] J. W. Rasul and T. Li, J. Phys. C **21**, 5119 (1988).

[21] T. Li, P. Wölfle, and P. J. Hirschfeld, Phys. Rev. B **40**, 6817 (1989).

[22] L. Lilly, A. Muramatsu, and W. Hanke, Phys. Rev. Lett. **65**, 1379 (1990).

[23] Hideo Hasagawa, Phys. Rev. B **41**, 9168 (1990), Prog. Theor.

Phys. Suppl. **101**, 463 (1990).
[24]W. Metzner and D. Vollhardt, Phys. Rev. Lett. **62**, 324 (1989).
[25]E. Müller-Hartmann, Z. Phys. B **74**, 507; **76**, 211 (1989).
[26]H. Schweitzer and G. Czycholl, Solid State Commun. **74**, 735 (1990).
[27]C. A. Balseiro, M. Avignon, A. G. Rojo, and B. Alascio, Phys. Rev. Lett. **62**, 2624 (1989).
[28]A. M. Olés and J. Zaanen, Phys. Rev. B **39**, 9175 (1989).
[29]Weiyi Zhang, M. Avignon, and K. H. Bennemann, Phys. Rev. B **42**, 10 192 (1990).
[30]E. N. Economou, *Green's Function in Quantum Physics* (Springer-Verlag, Berlin, 1979).
[31]M. F. Thorpe, in *Excitations in Disordered Systems,* edited by M. F. Thorpe (Plenum, New York, 1982), p. 85; F. Brouces *et al., ibid.,* p. 263.
[32]L. M. Falicov and F. Yudurain, Phys. Rev. B **12**, 5664 (1975); R. C. Kiltler and L. M. Falicov, J. Phys. C **9**, 4259 (1976).
[33]P. G. J. Van Dongen and D. Vollhardt, Phys. Rev. Lett. **65**, 1663 (1990).
[34]S. Engelsberg, W. F. Brinkman, and S. Doniach, Phys. Rev. Lett. **20**, 1040 (1968).
[35]S. Q. Wang, W. E. Evanson, and J. R. Schrieffer, Phys. Rev. Lett. **23**, 92 (1969); J. Appl. Phys. **41**, 1199 (1970).
[36]M. J. Zuckermann, Phys. Lett. **31** A, 362 (1970).
[37]M. Cyrot, J. Phys. **33**, 125 (1972); Philos. Mag. **25**, 1031 (1972).
[38]S. H. Liu, Phys. Rev. B **17**, 3629 (1978).
[39]J. Hubbard, Phys. Rev. B **19**, 2628 (1979).
[40]A. N. Andriotis, P. N. Poulopoulos, and E. N. Economou, Solid State Commun. **39**, 1175 (1981).
[41]J. Dorantes-Davila, J. L. Moran-Lopez, and M. Avignon, Phys. Rev. B **27**, 575 (1983).
[42]G. Baskaran, in *Progress in High Temperature Superconductivity, Trieste, Italy, 1988,* proceedings of the Adriatico Research Conference and Workshop on Towards the Theoretical Understanding of High T_c Superconductors, edited by S. Lundqvist, E. Tosatti, M. P. Tosi, and Yu Lu (World Scientific, Singapore, 1988), Vol. 14, p. 3.
[43]J. W. Rasul and T. Li, J. Phys. C **21**, 5119 (1988).
[44]M. Lavagna, Phys. Rev. B **41**, 142 (1990); Helv. Phys. Acta **63**, 310 (1990).
[45]J. Ferrer, F. Flores, E. Louis, A. Martin-Rodero, and J. A. Vergés, Phys. Rev. B **44**, 415 (1991).
[46]Note that this Green's function satisfies correctly $G_{(00)}(\omega\rightarrow\infty)=1/\omega$ and yields approximately correct density of states, the quasiparticle lifetime resulting from the interaction between quasiparticles not included in the calculation would only broaden the density of states.
[47]For comparison with other results in the limit $z\rightarrow\infty$, note that the limit $G_{(00)}(0)\rightarrow i/qt\sqrt{z}$ as $z\rightarrow\infty$ for the retarded Green's function should be taken for fixed bandwidth ($\sim\sqrt{z}\,t$).
[48]P. Fazekas, B. Menge, and E. Müller-Hartmann, Z. Phys. B **78**, 69 (1990).
[49]Y. Nagaoka, Phys. Rev. **147**, 392 (1966).
[50]P. W. Anderson, Phys. Rev. **115**, 2 (1959).
[51]F. C. Zhang and T. M. Rice, Phys. Rev. B **37**, 3759 (1989).
[52]D. Vaknin, S. K. Sinha, D. E. Moncton, D. C. Johnston, J. M. Newsam, C. R. Safinya, and H. E. King, Jr., Phys. Rev. Lett. **58**, 2802 (1987).
[53]C. Allgeier and J. S. Schilling, Physica C **168**, 499 (1990).